CHEMICAL ENGINEERING TRANSACTIONS
VOL. 119, 2025
A publication of AIDIC
The Italian Association of Chemical Engineering
Online at www.cetjournal.it
Guest Editors: David Bogle, Flavio Manenti, Piero Salatino

ISBN 979-12-81206-20-5; **ISSN** 2283-9216
DOI: 10.3303/CET25119026

Inline Mixing and Separation in a Tubular Reactor for Carbon Mineralization

Jairo Murillo-Rincon, Federico Alberini, Francesco Maluta, Alessandro Paglianti, Giuseppina Montante*

Department of Industrial Chemistry "Toso Montanari", University of Bologna, Bologna, Italy
giuseppina.montante@unibo.it

In this work, we investigate the fluid dynamics characteristics of a gas-liquid tubular reactor designed for the ex-situ continuous conversion of gaseous CO_2 into solid carbonates. The study consists in a combination of experiments and simulations concerning a pipe equipped with Kenics type static elements. The elements can be adopted for ensuring turbulent mixing and gas-liquid mass transfer or gas-liquid separation, depending on their relative orientation. In the experimental activity, we adopt optical and tomographic techniques to collect data on the bubbles size and the gas volume fraction distributions under different co-current gas-liquid flow conditions. The computational part of the work is based on the application of the Reynolds Averaged Two Fluid Model for the prediction of the gas-liquid flow characteristics, which affect the tubular reactor performances and the energy requirement. A preliminary analysis on the numerical errors, due to the spatial discretization of the computational domain close to the Kenics elements, is presented. The model evaluation based on the comparison of the simulation results with the experimental gas distribution highlights the current capability and limitations of Computational Fluid Dynamics based methodology for design, optimization and scale-up of the equipment.

1. Introduction

Inline tubular reactors are a highly promising alternative to batch reactors for a wide variety of applications, since they enable the design of continuous processes and allow for simultaneous reaction and separation with the same equipment. This approach aligns with the principles of process intensification in the chemical industry (Stankiewicz et al., 2019). Integrating reaction and separation in a single piece of continuous equipment can be particularly advantageous for ex situ aqueous mineral carbonation — the conversion of gaseous CO_2 into solid carbonates through its reaction with mineral oxides to form stable compounds (Gerdemann et al., 2007). Absorption and reaction of CO_2 in aqueous solution of dissolved minerals require turbulent mixing for the dispersion of fine bubbles in the liquid and the optimization of mass transfer rates. For turbulent gas-liquid mixing, tubular reactors equipped with static mixers can be adopted as an alternative to batch multiphase contactors, with appropriate design and optimization of the geometry (Altabash et al., 2023). Due to the significant density difference between the gas and liquid phases, the centrifugal forces generated in helical-type static elements can also facilitate phase separation (Rabha et al., 2015).
Innovative equipment for the continuous carbon mineralization can be designed by Computational Fluid Dynamics (CFD) based methods, provided that the modelling challenges related to the complex two-phase fluid dynamics are properly addressed and the uncertainties due to the numerical solution of the model equations in complex geometries are evaluated. Among the available multiphase flow models, the Euler-Euler Two Fluid Model (TFM) is nowadays widely adopted in a number of chemical engineering applications including gas-liquid static mixers (Zidouni et al., 2015) and it is also selected in this work. Since the bubble size distribution critically affects mass transfer and phase separation, it is experimentally measured together with the measured gas volume fraction distribution in the same system used for the simulations. The experimental data provide a physically grounded basis for selecting the appropriate sub-models in the TFM formulation and for evaluating the computational results.

Paper Received: 24 June 2025; Revised: 26 July 2025; Accepted: 12 October 2025
Please cite this article as: Murillo Rincon J., Alberini F., Maluta F., Paglianti A., Montante G., 2025, Inline Mixing and Separation in a Tubular Reactor for Carbon Mineralization, Chemical Engineering Transactions, 119, 151-156 DOI:10.3303/CET25119026

2. The investigated system

The investigation concerns a vertical pipe of diameter D equal to 0.022 m equipped with Kenics type static elements, as schematically depicted in Figure 1. The liquid and the gas phase are fed by separate inlets and they exit from a single outlet. Each static element consists of a twisted plate of diameter equal to D, length of 1.5 D and width equal to D/10. Depending on the twist angle, that is either 180° or -180° with respect to the pipe axis, each element provides clockwise or anticlockwise rotation to the flow. Depending on the type and arrangement of the elements, either mixing or separation of the two phases is obtained. The experimental results presented in the following and the pertinent simulations refer to the case of three elements located consecutively in the pipe at 10 D from the gas inlet and 17 D from the liquid inlet. The mixing and the separation configurations are investigated separately, with the three elements located in the pipe as depicted in Figure 1, either with alternating twist direction for obtaining mixing, or with the same twist direction for the separation. The fluids adopted in the experiments are water and air at ambient temperature. The gas-liquid flow characteristics are measured with a continuous flow rate of water and air of 943 L/h and 48 L/h, respectively. Correspondingly, the gas volume fraction is equal to about 5%, and the Reynolds number is 1.6×10^4, based on the pipe diameter, the mixture superficial velocity in the empty pipe, that is equal to 0.72 m/s, and the liquid physical properties. The bubble size distributions (BSD) are obtained from digital images analysed by the Shadow technique, as implemented in the Dantec Dynamics software DynamicStudio v7.6. The air volume fraction distributions are obtained from the Electrical Resistance Tomography (ERT) technique. The measurement locations are provided in Figure 1. Details on the Shadow and the ERT techniques as applied to similar systems have been reported by Alberini et al. (2024) and Yao et al. (2023), respectively.

The simulated domain matches quite closely the geometry of the experimental system, apart from the length of the pipe, that is equal to 35.5 D in the experiments. In the simulation, the length of the pipe upstream and downstream the Kenics is limited to 3 D and 7 D respectively, and the length of the three elements is equivalent to 4.5 D, resulting in a total length of 14.5 D. With the selected length of the computational domain, the computational cost is optimized without affecting the fluid dynamics characteristics of the two-phase flow obtained from the Kenics elements action. Also, in the simulation, a single inlet section for the two phases is considered, which is located at the lower cross section of the computational domain along the axial coordinate.

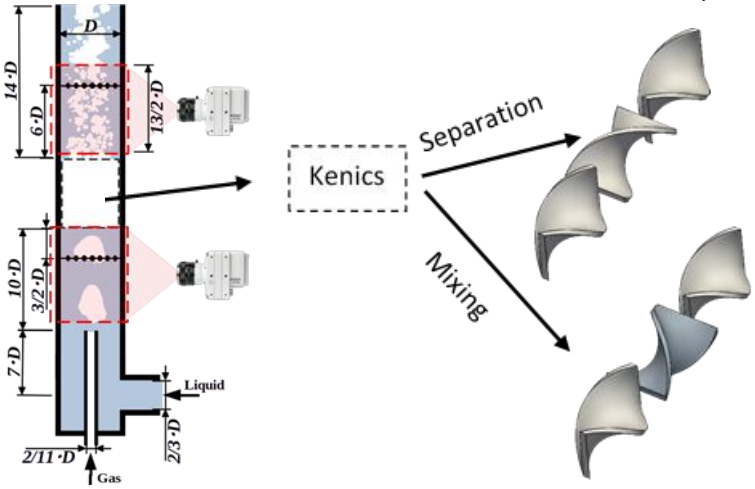

Figure 1: Sketch of the experimental system, location of the Shadow and ERT measurement sections and relative position of the Kenics elements for mixing and separation.

3. The model equations and the numerical solution method

The simulations of the turbulent gas-liquid flow are based on the numerical solution of the Reynolds Averaged Two Fluid Model equations implemented in OpenFOAM v11, that for the generic phase 'k' read:

$$\frac{\partial}{\partial t}(\alpha_k \rho_k) + \nabla \cdot (\alpha_k \rho_k \mathbf{u}_k) = 0 \tag{1}$$

$$\frac{\partial}{\partial t}(\alpha_k \rho_k \mathbf{u}_k) + \nabla \cdot (\alpha_k \rho_k \mathbf{u}_k \times \mathbf{u}_k) = -\alpha_k \nabla p + \nabla \cdot \left(\tau_k + \tau_k^t\right) + \alpha_k \rho_k \mathbf{g} + \mathbf{F}_{GL} \tag{2}$$

where α_k, ρ_k, $\mathbf{u}_k$, are the volume fraction, the density and the mean velocity vector of the phase 'k', p is the pressure, **g** is the gravity acceleration, τ_k and τ^t_k are the viscous and the Reynolds stress tensor, respectively,

and the subscript 'k' is replaced by 'L' for liquid phase and 'G' for the gas phase to indicate the momentum exchange forces between the liquid and gas phases, $\mathbf{F}_{GL}$.
The forces included in Eq(2) are the drag force, $\mathbf{F}_D$, and the turbulent dispersion force, $\mathbf{F}_{TD}$, arising from the time average of the drag force as derived by Burns et al. (2004), which sum reads:

$$\mathbf{F}_D + \mathbf{F}_{TD} = -\frac{3}{4}\frac{C_d \rho_L \alpha_G}{d_B}|\mathbf{u_G} - \mathbf{u_L}|\left[(\mathbf{u_G} - \mathbf{u_L}) + \frac{\nu_L^{turb}}{\sigma_{td}}\left(\frac{\nabla \alpha_G}{\alpha_G} - \frac{\nabla \alpha_L}{\alpha_L}\right)\right] \quad (3)$$

The bubble size, d_B, is taken equal to the experimental Sauter diameter downstream the static elements, that is equal to 2.3 mm in the mixing and 4.0 mm in the separation cases. The drag coefficient, C_d, is obtained from standard drag correlation of Ishii and Zuber, which covers a very wide range of conditions, as already reported by Zidouni et al. (2015). Swarm and liquid free stream turbulent effects on the drag coefficient are not taken into account. The turbulent Schmidt number, σ_{td}, is set to the standard value of 0.9, while the turbulent viscosity, ν_L^{turb} is obtained from the turbulence model. Additional forces are neglected. The magnitude of the virtual mass, $\boldsymbol{F}_{VM}$, lift, $\boldsymbol{F}_L$, and wall lubrication, $\boldsymbol{F}_{WL}$, forces is estimated a-posteriori using the classical definitions, that read:

$$\mathbf{F}_{VM} = -0.5\rho_L \alpha_G \left(\frac{D_G \mathbf{u}_G}{Dt} - \frac{D_L \mathbf{u}_L}{Dt}\right) \quad (4)$$

$$\mathbf{F}_L = -0.288\rho_L \alpha_G (\mathbf{u}_G - \mathbf{u}_L) \times \nabla \times \mathbf{u}_L \quad (5)$$

$$\mathbf{F}_{WL} = \frac{2}{d_B} 0.5791 \rho_L \alpha_G |\mathbf{u}_G - \mathbf{u}_L|^2 \hat{y} \quad (6)$$

where D_G/D_t and D_L/D_t are the material derivatives with respect to the velocity of each phase, $\hat{y}$ is unit vector normal to the wall pointing into the fluid.
The Reynolds stress tensor τ_k^t, is obtained adopting the Boussinesq approximation and the turbulent viscosity is obtained by the single phase k - ω turbulence model applied to the two-phase flow by adopting the mixture properties of the phases, corresponding to the following model equations:

$$\frac{\partial k_m}{\partial t} + \nabla \cdot (\boldsymbol{u}_m k_m) - \nabla \cdot (D_{eff,k_m} \nabla k_m) = P_m - 0.09\omega_m k_m + S_k \quad (7)$$

$$\frac{\partial \omega_m}{\partial t} + \nabla \cdot (\boldsymbol{u}_m \omega_m) - \nabla \cdot (D_{eff,\omega_m} \nabla \omega_m) = 0.52 P_m \frac{\omega_m}{k_m} - 0.072\omega_m^2 + S_\omega \quad (8)$$

where k_m is the turbulent kinetic energy, $\omega_m$is the specific dissipation rate of turbulent kinetic energy, P_m is the production term, S is the source term and D_{eff} is the effective diffusivity. At the boundary of the domain, the following conditions are set. On the walls a no-slip condition and a free-slip condition are imposed for the liquid and the gas respectively. As for the near-wall treatment, it is based on the formulation of Menter et al. (2003) that shifts gradually between a viscous sublayer formulation and wall functions. At the inlet, the gas volume fraction is set equal to 5%, the turbulence intensity of 0.02 % is assigned based on an empirical correlation for pipe flows, the velocity profile of a fully developed turbulent flow in a straight pipe is set for both phases, matching with the experimental volumetric flow rate. At the outlet, the static pressure is set equal to the atmospheric pressure. The simulation is initialized in the whole domain with the average mixture superficial velocity 0.72 m/s for both phases, a uniform distribution of 5% gas volume fraction, almost nil values for the turbulent kinetic energy and the specific turbulent dissipation rate and atmospheric pressure.
The resulting set of equations is solved by the multiphaseEulerFoam solver, adopting second order discretization scheme for the convective terms and the Local Time Stepping approach (LTS) for the temporal solution strategy using a first order scheme. The pressure-velocity coupling is based on the PIMPLE algorithm. The time steps were restricted to maximum values of $1\text{x}10^{-4}$ s with a maximum Courant number of 0.3. In addition to the residuals monitoring, the achievement of the solution is estimated monitoring the velocity and the gas volume fraction in selected locations of the domain.
Preliminary single phase flow simulations are performed to separately evaluate the effect of the spatial discretization of the computational domain on the liquid mean flow and turbulent characteristics. The single phase results are obtained from the solution of the Reynolds Averaged Navier Stokes equations and the single phase version of the $k-\omega$ turbulence model by the pimpleFoam OpenFOAM solver.

3.1 Grid dependence

The evaluation of the grid convergence is based on the comparison of the numerical results obtained in single phase flow with one static element in the pipe and three structured grids built with the Gmsh software. Focusing on the discretization of the fluid volume bounded between the element and the pipe wall, the average size of

the cells is reduced with a factor of 1.3, as reported in Table 1, where also the minimum and the maximum value of the near wall resolution in wall units, y^+, for the pipe wall is given.

Table 1: Number of cells and y^+ at the pipe wall for the three grids adopted in the grid convergence study

	Grid 1	Grid 2	Grid 3
$z \times r \times \theta$	86×50×120	116×66×152	158×86×192
y^+_{min}	5.70×10^{-7}	5.78×10^{-7}	5.74×10^{-7}
y^+_{max}	14.71	16.85	14.38

The three meshes on the wall of the static element are shown in Figure 2 with the value of y^+ depicted as color map.

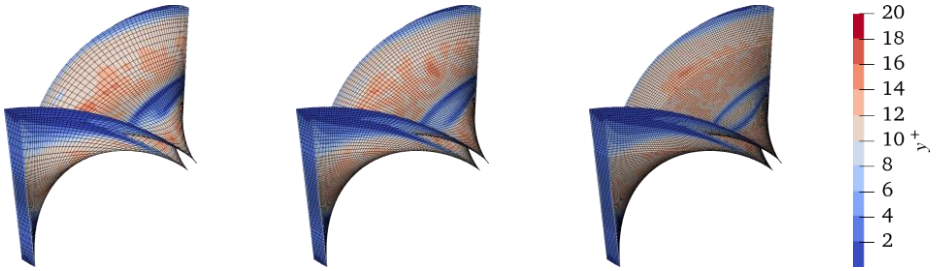

Figure 2: Mesh on the static element wall and color map of y+ for Grid 1 (a), Grid 2 (b) and Grid 3 (c).

Selected results obtained with the three grids just downstream the mixers are shown in Figure 3, in a diametrical plane portion located along the pipe axis (Figures 3a and 3b) and on a cross section (Figures 3c and 3d). The mean velocity is shown in Figures 3(a) and 3(c) and the turbulent kinetic energy dissipation rate is shown in Figure 3(b) and 3(d).

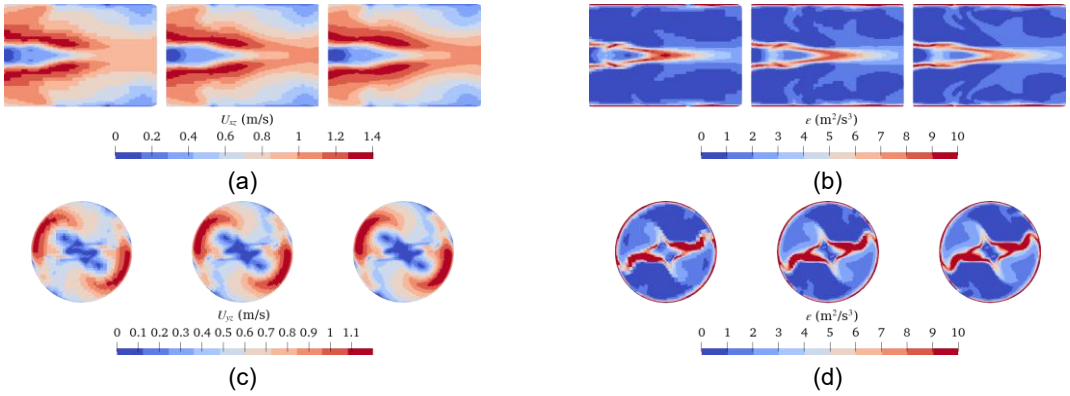

Figure 3: Maps of in-plane components of the velocity magnitude (a, c) and turbulent kinetic energy dissipation rate (b, d) with increasing grid refinement downstream the elements.

The grid refinement has a visible effect moving from Grid 1 to Grid 2, although both the mean and the turbulent variable variations are not marked, and minor differences can be observed on the selected planes with the two finer grids. Also, the integral value of the turbulent dissipation rate over the whole computational domain is equal to 4.8, 5.1, 5.2 m^2/s^3 respectively moving from the coarse to the finer grid, with the maximum deviation from the integral value obtained from the Richardson extrapolation of 5.3 equal to 7%. Based on a detailed analysis performed in a previous work for a similar system in single phase flow conditions (Murillo-Rincon et al., 2025), the two-phase flow simulations are carried out with Grid 3. Additional analysis of the grid effect on the TFM results will be presented in future works.

4. Results and discussion

The BSD measured just after the gas inlet and downstream the Kenics in the mixing and the separation arrangements are shown in Figure 4(a). For each case, a raw digital image of the bubbles and the map of gas hold-up measured by ERT on the pipe cross sections are also shown in Figure 4(b).

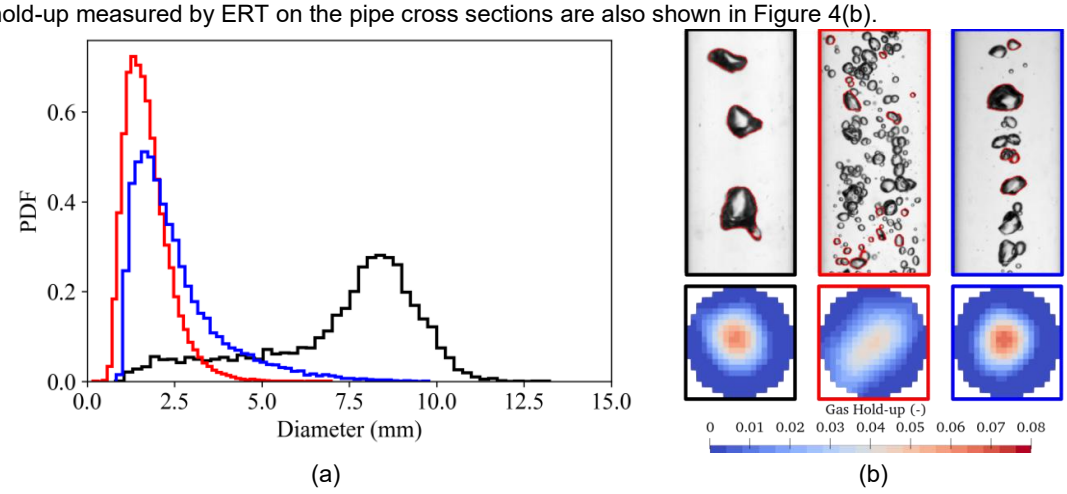

Figure 4: (a) BSD downstream the Kenics in the mixing (red line), separation configuration (blue line) and after the gas inlet (black line). (b) Digital image and map of the gas hold-up in a box of the same colour of the corresponding BSD. The ERT plane location is 33 mm upstream (black box) or 132 mm downstream the elements (red and blue box).

The effectiveness of the Kenics in both the mixing and the separation tasks is apparent. Much smaller bubbles with respect to the initial size are obtained in the mixing arrangement and they are spread relatively well in the cross section. In the separation configuration, the Kenics action reduces the bubble size less with respect to the mixing configuration and gas segregation in the central region of the pipe is obtained. The experimental Sauter diameters are adopted for the gas-liquid simulations to evaluate the appropriateness of the interphase momentum transfer terms which are required in the TFM for a realistic prediction of the gas dispersion and segregation. The simulation results for the mixing case are shown in a diametrical cross section along the pipe axis in Figure 5.

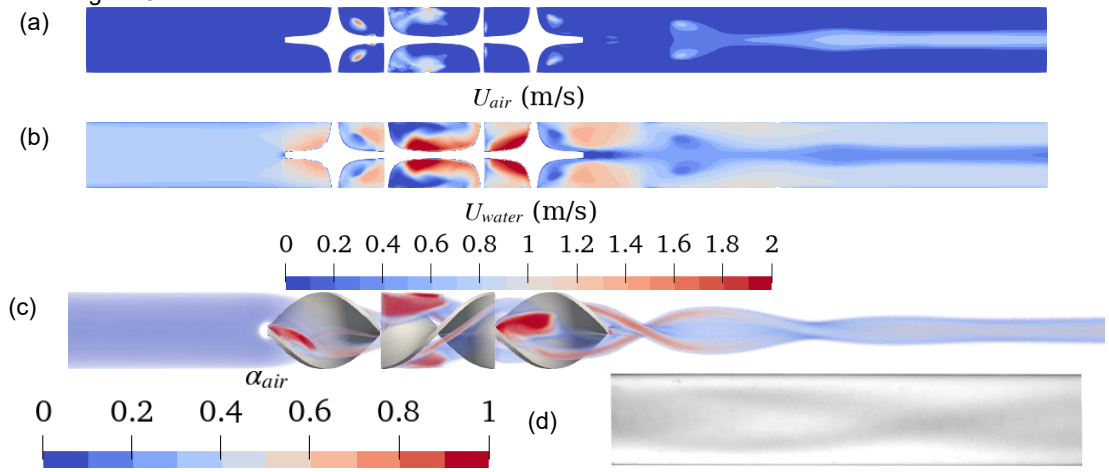

Figure 5: Gas (a) and liquid (b) velocity magnitude, gas volume fraction distribution (c) and mean experimental image (d).

The spatial inhomogeneity of the velocity magnitude along the pipe length shown in Figure 5(a) and (b) for the gas and the liquid phase respectively highlights the usefulness of the local description of the flow variable in the reactors with respect to concentrated parameter models. The distribution of the gas volume fraction shown in Figure 5(c) exhibits features similar to the mean experimental image of the bubbles (Figure 5d), although in the simulation the bubbles distribution on the pipe section appears less uniform.

Based on the a posteriori calculation shown in Figure 6, improvement in the model predictive capability can be expected accounting for the virtual mass and lift interphase forces, while the contribution of the wall lubrication force appears negligible. Different formulations of the turbulent dispersion force may also be worth of further evaluation, provided that it should provide a major contribution to the bubble dispersion in the pipe cross section.

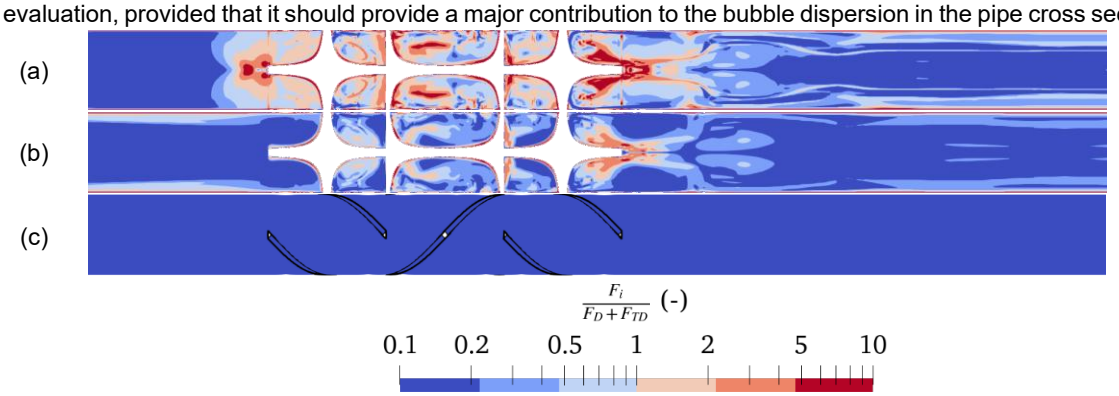

Figure 6: Magnitude of forces not included in Eq(2) divided by the magnitude of the drag and turbulent dispersion force (a) Fi= FVM; (b) Fi= FL; (c) Fi= FWL.

5. Conclusions

In this work, a novel application of Kenics type static elements for obtaining gas-liquid mixing and separation within the same equipment has been proposed and original data have been presented. A modelling method based on the TFM as implemented in the CFD code OpenFOAM was adopted. A fair prediction of the gas-liquid fluid dynamics was obtained from the simulations based on the experimental bubble Sauter diameter. The investigation has provided a sound basis towards a comprehensive modelling method that will include the bubble breakage, the gas-liquid mass transfer and the chemical reaction kinetics for the prediction of the capacity and the energy requirement for the mineralization of CO_2 in a continuous operation.

Acknowledgments

We acknowledge the CINECA award under the ISCRA initiative, for the availability of high performance computing resources and support.

References

Alberini F., Nerini F., Mandolini N., Maluta F., Paglianti A., Pasquale N.D., Montante G., 2024, On the reliability of image analysis for bubble size distribution measurements in electrolyte solutions in stirred reactors, Chemical Engineering Journal Advances, 20, art. no. 100658.

Altabash G., Al-Hindi M., Azizi F., 2023, Intensifying the Absorption of CO2 in Water Using a Static Mixer; Part II: Effect of Reactor Design, Industrial and Engineering Chemistry Research, 62, 13612 – 13626.

Burns, A. D., Frank, T., Hamill, I., & Shi, J. M., 2004, The Favre averaged drag model for turbulent dispersion in Eulerian multi-phase flows, 5th international conference on multiphase flow, ICMF (Vol. 4, pp. 1-17). ICMF.

Gerdemann S.J., O'Connor W.K., Dahlin D.C., Penner L.R., Rush H., 2007, Ex situ aqueous mineral carbonation, Environmental Science and Technology, 41, 2587-2593.

Menter, F., Ferreira, J. C., Esch, T., & Konno, B., 2003, The SST turbulence model with improved wall treatment for heat transfer predictions in gas turbines, Gas Turbine Congress (International) Proceedings. Tokyo. Paper No. *Tokyo. Paper*, (IGTC2003), 059.

Murillo-Rincon J., Maluta F., Alberini F., Paglianti A., Montante G., 2025, Computational modelling of the fluid dynamics in a tubular reactor equipped with different static element configurations, Physics of Fluids, 37, 025181.

Rabha S., Schubert M., Grugel F., Banowski M., Hampel U., 2015, Visualization and quantitative analysis of dispersive mixing by a helical static mixer in upward co-current gas-liquid flow, Chemical Engineering Journal, 262, 527 – 540.

Stankiewicz A., Van Gerven T., Stefanidis G., 2019, The Fundamentals of Process Intensification, ISBN: 978-3-527-32783-6, Wiley-VCH, Weinheim.

Yao Z., Alberini F., Montante G., Paglianti A., 2023, In-line monitoring of mixing performance for smart processes in tubular reactors, Chemical Engineering Research and Design, 194, 678 - 692

Zidouni F., Krepper E., Rzehak R., Rabha S., Schubert M., Hampel U., 2015, Simulation of gas-liquid flow in a helical static mixer, Chemical Engineering Science, 137, 476 – 486.